

Evolution of a tide-dominated abandoned channel: A case of the abandoned Qingshuigou course, Yellow River

Xiao Wu^{a,b,*}, Houjie Wang^{a,b}, Naishuang Bi^{a,b}, Jeffrey A. Nittrouer^c, Jingping Xu^{b,d}, Shuai Cong^a, Brandee Carlson^c, Taian Lu^a, Zhaoying Li^{a,c}

^a College of Marine Geosciences, Key Laboratory of Submarine Geosciences and Prospecting Technology, Ocean University of China, 238 Songling Road, Qingdao 266100, China

^b Laboratory for Marine Geology, Qingdao National Laboratory for Marine Science and Technology (QNLN), 1 Wenhai Road, Qingdao 266061, China

^c Department of Earth, Environmental and Planetary Sciences, Rice University, 6100 Main Street, Houston, TX 77005, USA

^d Department of Ocean Science & Engineering, Southern University of Science and Technology, 1088 Xueyuan Road, Shenzhen 518055, China

ARTICLE INFO

Editor: Shu Gao

Keywords:

Abandoned river channel
Yellow River delta
Geomorphic evolution
Sedimentary sequence

ABSTRACT

Deltaic river systems including both active channels and abandoned channels, are of significant importance to understand the deltaic morphology, as well as to the coastal management and ecosystem maintenance. However, the healing process of the abandoned channel has not yet been well understood. Based on the sedimentary record and hydrographic surveys, the deposit architecture and sediment dynamics of a tide-dominated abandoned channel, the abandoned Qingshuigou channel of the Yellow River, are investigated. The abandoned Qingshuigou channel has been fully disconnected from the main river channel since an artificial diversion completed in 1996. Twenty years after the abandonment, sedimentation with an average thickness of > 20 cm was identified in the abandoned channel, illustrating a prominent seaward thickening trend from middle to lower channel. At the present river mouth of the abandoned channel, sedimentation layer with a thickness of 38 cm well matched the sedimentation rates derived from both chronological framework (1.85 cm/yr derived from ²¹⁰Pb) and sedimentary facies (1.90 cm/yr). These deposits are composed by fine-grained sediment and enriched with organic matters, differing largely from the river-dominated deposits before abandonment. Tidal delivery of the sediment resuspended in the shallow water nearby Qingshuigou river mouth dominated the refilling process of the abandoned channel. Meanwhile, severe erosion near the abandoned river mouth shortened the channel (23.5 km in 1996 versus 14.5 km in 2018) and induced a lateral migration of the tidal inlet. Due to seasonally varying hydrodynamics, the tide-dominated abandoned Qingshuigou channel converts from a sediment sink in summer seasons to both a source and a sink in winter seasons.

1. Introduction

A river is natural conduit for water as it drains a catchment and delivers sediment to a receiving basin, such as ocean, sea, lake or possibly another river (Wetzel, 2001). With a total global surface area of ~773,000 km², rivers are largely transboundary and connect a considerable proportion of continental surface (Bakker, 2009; Allen and Pavelsky, 2018). From watershed scale to global scale, and over days to millions of years, rivers continually shape the Earth's landscape through deposition, erosion and redistribution of terrestrial sediment (Best, 2019). Large amount of terrestrial sediment was transported into the ocean by rivers and accumulated near their initial sites of entry into the sea, forming various deltas. Deltas are presently important to sustain

global society and economy, but they are highly threatened by sea-level fluctuation, land subsidence, and sediment supply (Syvitski et al., 2009; Syvitski and Saito, 2007). Continuous drowning of deltas in recent decades makes it more urgent than ever to better understand delta evolution at varying scales. As an essential component of delta and indispensable vehicle for transporting sediment, deltaic river systems and their evolution have thus been considered as an important issue for insightful understanding of delta evolution (Gugliotta and Saito, 2019).

Deltaic river systems are generally comprised of three types of river channels: (1) active channel; (2) abandoned channel which partially connect with main channel; and (3) abandoned channel which is fully disconnected from the main channel. The first two types have been studied extensively in recent years (e.g. Dai et al., 2016; Gray et al.,

* Corresponding author at: College of Marine Geosciences, Key Laboratory of Submarine Geosciences and Prospecting Technology, Ocean University of China, 238 Songling Road, Qingdao 266100, China.

E-mail address: wuxiao@ouc.edu.cn (X. Wu).

<https://doi.org/10.1016/j.margeo.2020.106116>

Received 2 September 2019; Received in revised form 29 December 2019; Accepted 2 January 2020

Available online 14 January 2020

0025-3227/ © 2020 Elsevier B.V. All rights reserved.

2016; Gugliotta et al., 2017; Ogston et al., 2017; Gugliotta and Saito, 2019). The hydrological condition and geomorphic evolution of these channels are controlled by the battle of fluvial process and tide-dominated regime of the open coast (Ogston et al., 2017). Near the receiving basin, where tidal forcing is dominant, distributary channels typically increase in width and decrease in depth with proximity to the sea. Distributary channel beds in this region display tide-influenced sand-mud alternations (Gugliotta and Saito, 2019). Meanwhile, due to strong tidal currents and insufficient sediment supply, more erosional features potentially occurred near river mouth areas in recent years (e.g. Dai et al., 2016; Gugliotta et al., 2017). However, very few studies have focused on the third type (i.e. deltaic channels which fully disconnect from the main channel), except for an ideal model hypothesized by Gugliotta and Saito (2019). In their so-called ‘purely tide-dominated channel’, sediment eroded near the tidal inlet would be transported landward, resulting in the gradual infilling of the channel. To the best of our knowledge, however, this assumption has not been verified or falsified by any practical cases. As a consequence, the sedimentary architecture in these abandoned channels also remains unclear. As deltas play a major role in sustaining society (e.g., providing fertile soil, abundant natural resources, and settlement to half a billion people worldwide; Syvitski and Saito, 2007; Iglesias-Campos et al., 2015), better understanding these purely tide-dominated abandoned channels as a component to the general geomorphic evolution of deltas is of critical importance (Gray et al., 2018).

The Yellow River is well known for its heavy sediment load and fast deltaic land accretion (Xue, 1993; Saito et al., 2001; Wang et al., 2010). Given the high sediment load and relatively low water discharge, the sediment is mostly deposited on the lower riverbed and raises the channel bed, forming a “suspended river” in the lower reaches of the Yellow River (Wang et al., 2017). The channel levees and channel bed are highly elevated, even in delta regions. Therefore, water depth of the lower reaches is relatively shallow and backwater length is short (e.g. channel bed elevation at 40–50 km upstream from the river mouth is ~3 m in 1997; Wu et al., 2017). The perched channels are fragile to flash floods and therefore have forced the lower Yellow River to meander within its flat delta plain (Fig. 1a). Frequent avulsions provide a good opportunity to study the evolution of abandoned channel. At

millennial scale, the Yellow River empties into the micro-tidal Bohai Sea, forming river-dominated deltas along the western coast of the Bohai Sea due to the frequent channel avulsions in the lower reaches (Saito et al., 2001). But at the end of the river channel, tidal processes also could impact channel morphology and tend to widen deltaic channels (Fig. 1b; Gugliotta and Saito, 2019). Especially, the Yellow River was artificially diverted northward from the Qingshuigou course to the Qing 8 course in 1996 (Fig. 1b). Since then, the Qingshuigou course has been completely cut off and fully disconnected from the main channel by man-made dyke. Without connection with the main river channel, the abandoned Qingshuigou channel was converted into a purely tidal end-member system as hypothesized by Gugliotta and Saito (2019).

Herein, based on sediment cores collected on the abandoned Qingshuigou channel and time-series hydrographic surveys in the abandoned river mouth, we discussed the morphological evolution of Qingshuigou channel after abandonment. The objective of this work is to identify the nature of the sedimentary deposit, and infer the filling dynamics of an abandoned channel influenced by ocean dynamics. By comparing to the infilling process of deltaic channels influenced by both tidal and fluvial processes, the differences in the evolutionary processes for the two unique settings are addressed in detail. The insights gained in this paper have important implications to the infilling processes of abandoned channels in river deltas, specifically by clarifying controlling factors. A better understanding of the abandoned channel development in deltaic morphology system is also critical for coastal management and ecosystem maintenance, which are ever-more pressing given the growing risk of coastal erosion induced by the combined impacts from climate change and human activity (Syvitski et al., 2009).

2. Study area

Originating from the northern Qinghai-Tibetan Plateau, the Yellow River flows eastward through the Loess Plateau and the North China plain with a length of 5464 km, before entering the shallow and semi-closed Bohai Sea. Historically, over 1.6×10^9 tons of sediment from the Loess Plateau is delivered to the lower reaches annually (Shi et al.,

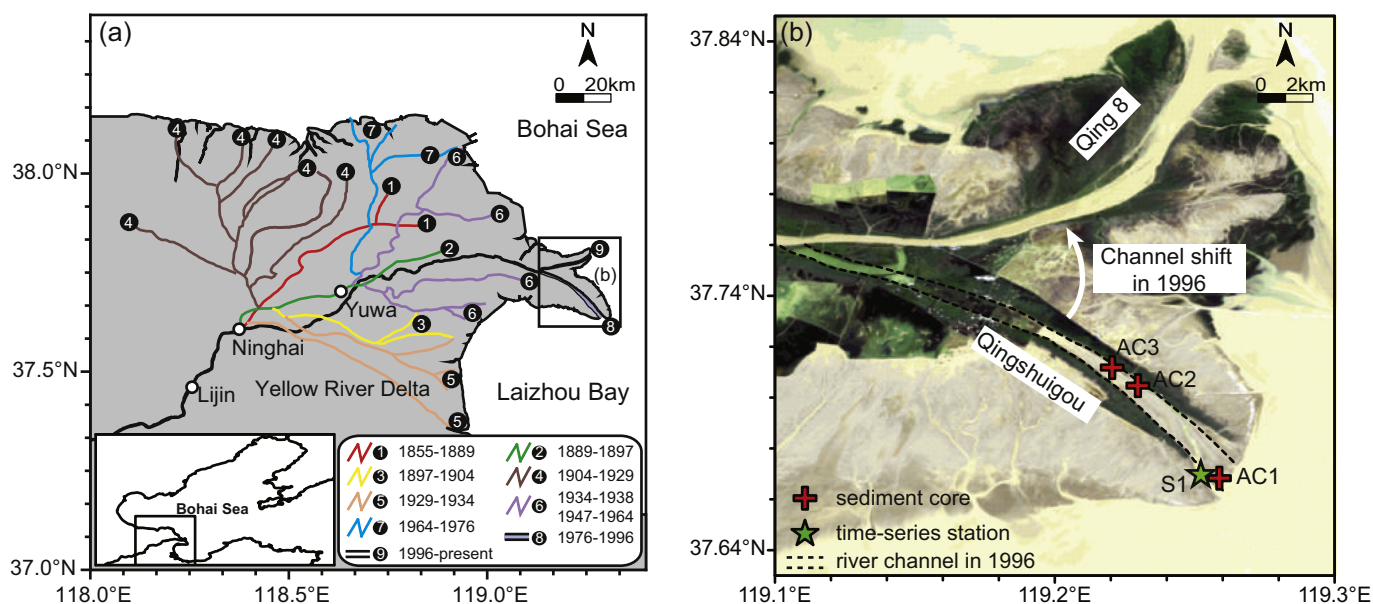


Fig. 1. (a) Historical channel shifts of the lower Yellow River since 1855 (modified after Xue, 1993); (b) map of the abandoned Qingshuigou river channel with sampling stations: core AC1 (37.67°N, 119.26°E, 0.40 m), core AC2 (37.70°N, 119.23°E, 0.68 m), core AC3 (37.71°N, 119.22°E, 0.70 m), and time-series station S1 (37.68°N, 119.25°E). The dash line indicates the river channel in 1996. Red crosses and green stars are locations of sediment cores and the time-series station, respectively. The elevation data is from Shuttle Radar Topography Mission (SRTM) datasets. (For interpretation of the references to colour in this figure legend, the reader is referred to the web version of this article.)

2002). Due to its high sediment concentration and relatively low water discharge, coarse-grained sediment deposits on the riverbed, forming a 'suspended river' in its lower reaches, whereby the channel bed is highly elevated above the surrounding floodplain (Wang et al., 2017; Bi et al., 2019). Such a perched channel and high sediment load renders the system dynamic insofar that floods and crevasses (levee breaches) have caused the Yellow River to meander and avulse over much of its wide and flat alluvial plain for the past several thousand years (Saito et al., 2001). Since 1855, when the Yellow River avulsed northward from the North Jiangsu Province to the northern side of the Shandong Peninsula, the deltaic section of the river channel has itself avulsed approximately 9 times (Fig. 1a). As a result of relocating the delta depositional center, approximately 5400 km² of subaerial deltaic landscape has formed in the past ~150 years (Xue, 1993). Therefore, the channels of the lowermost Yellow River provide a good opportunity to investigate the geomorphic evolution of abandoned river deltaic channels in general.

The modern Yellow River delta today nourishes more than two million people, supporting their livelihoods, which includes farming, aquaculture, fishing, and the second largest oil field (i.e. Shengli Oilfield) in China (Zhou et al., 2015). Besides fast land accretion, frequent avulsions of the deltaic river channels have also caused inundation disasters and impeded local economic development. In response, artificially designed avulsions have been applied to the lower Yellow River reaches since the 1950s (Zheng et al., 2018). Furthermore, in order to facilitate infrastructure construction of the Shengli Oilfield, the Yellow River was artificially diverted northward from the Qingshuigou course to the Qing 8 course in 1996 (Fig. 1b). Since then, the Qingshuigou course has been completely cut off and dynamically disconnected with the main channel by man-made dyke.

The abandoned Qingshuigou channel is approximately 20 km long and located in eastern end of the modern Yellow River delta (Fig. 1b). The tidal regime of the abandoned river mouth is dominated by a mixed semi-diurnal tide with a range of 0.6–0.8 m. The tidal currents generally flow parallel to the isobaths: northward/southward during the flood/ebb tide, respectively, with an average current speed of 0.2–0.6 m/s (Zhang et al., 1990; Bi et al., 2010). The climate in the study area maintains a distinct seasonal variability associated with East Asian Monsoon activity. A weak southerly wind prevails in summer, while a stronger northerly wind with an average speed > 10 m/s dominates during the winter seasons. The waves in the study area are mostly driven by the local winds, of which the dominant northerly waves in winter are much stronger than the southerly waves in summer (Wang et al., 2014).

3. Materials and methods

3.1. Sampling

A total of three sediment cores with lengths of 100 cm (AC1), 43 cm (AC2), and 50 cm (AC3) were collected in the abandoned Qingshuigou channel using a vibracore set. The sites of cores AC1, AC2 and AC3 were progressively landward in the abandoned channel (Fig. 1b). It is noteworthy that these three cores were collected in different years. Core AC1 was firstly collected near the abandoned river mouth in July 2015 and was sampled every 1 cm for grain-size analysis in the laboratory. Additionally, based on the sedimentary sequence, 10, 14 and 10 sediment samples at selected depth (every 5 or 10 cm) of core AC1 were taken for measurements of radionuclides ²¹⁰Pb concentration, organic carbon and straight chain alkanes (n-alkanes) data, respectively. These data are critical to interpret the geomorphic evolution of the abandoned channel, as they provide constraints on accumulation rates and origin (marine, terrestrial) of organic material for the sedimentary deposit.

Core AC1 provided a preliminary understanding on the vertical sedimentary structure. Subsequently, cores AC2 and AC3 were then collected in July 2018, in order to distinguish the spatial variation of

the channel filling architecture. Cores AC2 and AC3 also presented similar patterns to core AC1, insofar that both cores show two segments that differ largely from each other. These cores were also sectioned at 1 cm intervals for grain-size analysis.

3.2. Analytical procedures

All sediment samples of three cores were pretreated with 30% H₂O₂ to decompose organic matter and 1 mol/l HCl to remove carbonate. After dispersion and homogenization by ultra-sonic vibration, the grain size of the sediment samples was measured using a laser particle size analyzer (Mastersizer 2000, Malvern Instruments Ltd., UK) with a measuring error of < 3%. The particle sizes were categorized into three fractions: clay (< 4 μm), silt (4–63 μm), and sand (> 63 μm).

The ²¹⁰Pb dating of core AC1 was conducted at the Third Institute of Oceanography, Ministry of Natural Resources, based on the method outlined in Guo et al. (2007). After air-drying and pulverization, the powdered samples were measured by an Ortec HPGe GWL series well-type coaxial low background intrinsic germanium detector. ²¹⁰Pb was determined by gamma emissions at 46.5 keV, while ²²⁶Ra was determined via the gamma emission of its daughter isotope ²¹⁴Pb at 295 keV and 352 keV, following three weeks of storage in sealed containers to attain radioactive equilibration. The excess ²¹⁰Pb (²¹⁰Pb_{ex}) was calculated by subtracting ²²⁶Ra activity from total ²¹⁰Pb activity. The sedimentation rate was calculated from the logarithmic regression profile of ²¹⁰Pb_{ex} versus depth by the constant initial concentration model (Guo et al., 2007).

Analyses of total organic carbon (TOC) and n-alkanes of selected sediments of core AC1 were performed at the First Institute of Oceanography, Ministry of Natural Resources. Portions of the freeze-dried sediment samples were pretreated with 4 M HCl to remove carbonate, and the resulting carbonate-free samples were then analyzed for TOC in duplicate using a Vario EL-III Elemental Analyzer. To determine n-alkanes, approximately 15 g of freeze-dried sediments were extracted with dichloromethane in a Soxhlet apparatus for 48 h, with activated copper added to remove the sulfur in the samples. The extracts were concentrated by rotary evaporation, hexane-exchange, and submitted to a 1:2 alumina/silica gel glass column. The subsequent fraction containing aliphatic hydrocarbons was eluted and reduced in volume using a gentle N₂ stream. Then the extract was added with a known quantity of hexamethylbenzene as internal standard. After pre-treating, data of n-alkanes were measured by an Agilent 6890 Series Gas Chromatography/Series 5975 Mass Spectrometer in the full scan mode, and chromatographic separation was achieved by DB-5MS capillary column, following the detailed procedures described in Hu et al. (2009). The carbon preference index (CPI), terrigenous/aquatic ratios (TAR) and light/heavy ratios (L/H) are useful indices for distinguishing terrigenous and marine sediments (Meyers, 1997; Hu et al., 2013; Liu et al., 2018). The CPI, TAR and L/H values are defined as follows (Bray and Evans, 1961; Aboul-Kassim and Simoneit, 1996; Meyers, 1997; Liu et al., 2018).

$$CPI = \left(\frac{1}{2} \right) \left(\frac{nC_{25} + C_{27} + C_{29} + C_{31} + C_{33}}{nC_{26} + C_{28} + C_{30} + C_{32} + C_{34}} + \frac{nC_{25} + C_{27} + C_{29} + C_{31} + C_{33}}{nC_{24} + C_{26} + C_{28} + C_{30} + C_{32}} \right) \quad (1)$$

$$TAR = \frac{nC_{27} + nC_{29} + nC_{31}}{nC_{15} + nC_{17} + nC_{19}} \quad (2)$$

$$\frac{L}{H} = \frac{\sum_{n=14}^{23} C_n}{\sum_{n=24}^{33} C_n} \quad (3)$$

3.3. Hydrographic surveys

Time-series hydrographic surveys in the abandoned river mouth (station S1, Fig. 1b) were conducted on August 06, 2017 and March 15–16, 2018, respectively, to distinguish the sediment transport in summer and winter seasons. The water depth was extremely shallow with variations of 1–3 m during the flood/ebb tide. As a result, the surveys were only conducted by using a small fishing-boat due to the limitation of draught. Thus the time-series data of current velocity and turbidity were only obtained at 1 m below the surface using electromagnetic current meter and RBR turbidity sensor. Water samples of 500 ml were collected at the corresponding position with a time interval of 1 h. Water samples were then filtered through pre-weighed paired filters 47 mm in diameter with a pore diameter of 0.45 μm . The filters with sediments were washed three times with distilled water to remove the remaining salt. The dried filters were weighed again using a high-resolution electronic balance with an accuracy of 0.01 mg. The suspended sediment concentration (SSC), calculated from the ratio of the mass of final filtered sediment to filtered water volume, was used to validate the turbidity data. The horizontal suspended sediment flux (SSF) at station S1 was calculated based on flow vector and turbidity-derived SSC.

$$SSC = 0.95 \times TU - 3.71 \quad (R^2 = 0.91, n = 38). \quad (4)$$

$$SSF_{U(V)} = SSC \times U(V) \times H. \quad (5)$$

$$|SSF| = \sqrt{SSF_U^2 + SSF_V^2}. \quad (6)$$

U and V represent the eastward and northward components of current velocity measured at 1 m below the surface, respectively. H is the water depth (i.e. the mean water depth of 2 m used in here).

3.4. Satellite images

Multi-temporal remote sensing data of Landsat Thematic Mapper (TM) and Landsat Enhanced Thematic Mapper (ETM+) satellite images from 1996 to 2013 were acquired from the Earth Resources Observation and Science (EROS) Center (<http://glovis.usgs.gov/>). Each full TM or ETM+ scene can fully cover the study area with the spatial resolution of 30 m. The central endpoints of the abandoned Qingshuigou river mouth in different years were extracted based on the middle of estuary derived from acquired Landsat imageries.

4. Results

4.1. Spatial evolution of the abandoned Qingshuigou channel

As indicated by time-series satellite images, the abandoned Qingshuigou course has shrunk significantly since the artificial diversion in 1996 (Fig. 2). The abandoned river mouth retreated landward successively (Figs. 2 and 3). For instance, the site of core AC1, which was collected on land in 2015, has been already submerged in 2018 (Fig. 2f). Correspondingly, the channel length was shortened from 23.5 km in 1996 (Fig. 2a) to 14.5 km (Fig. 2f) in 2018, with an average shortening rate of 0.4 km/yr. Besides, the tidal channel that currently occupies the abandoned channel was much shorter than the antecedent fluvial channel (Fig. 2), indicating that obvious channel infilling has actually occurred in the whole abandoned channel, from the man-made dyke to abandoned river mouth. Only the center of the abandoned channel remained a subaqueous environment nowadays (Fig. 2). Meanwhile, severe erosion of the west bank, along with accretion of the east bank, occurred near the abandoned river mouth, inducing a lateral migration of the tidal inlet (Fig. 3).

4.2. Sedimentary sequence of the abandoned Qingshuigou channel

4.2.1. Chronological framework of Core AC1

Based on sedimentary features, core AC1 can be distinctly divided into two segments (0–38, 38–100 cm): sediments in the upper 38 cm were dominantly composed by yellowish-gray clayey silt. Grayish-yellow silty sand and sandy silt were found in the lower segment below 38 cm. A few black stripes were found occasionally in the sequence. For conditions that sediment is muddy and steadily accumulated, ^{210}Pb is considered as a reliable age-dating proxy. Generally, if $^{210}\text{Pb}_{\text{ex}}$ decreases downward with depth, this indicates that the sediment accumulated at a relatively constant rate in a stable sedimentary environment. As shown in Fig. 4, a distinct break in the $^{210}\text{Pb}_{\text{ex}}$ profile of core AC1 was found, corresponding to a distinct interruption in the sedimentary sequence. The ^{210}Pb data of the lower segment seemed to be not applicable due to sandy silt deposits. Thus only ^{210}Pb data of the upper segment was used. The $^{210}\text{Pb}_{\text{ex}}$ profile of the upper 38 cm of core AC1 showed a stable downward decreasing trend in the activity of $^{210}\text{Pb}_{\text{ex}}$, and a best-fit linear regression with a correlation coefficient $R = 0.75$, which yielded an estimate of average sedimentation rate of 1.85 cm/yr. Therefore, the upper segment (0–38 cm) corresponded to the sedimentation within approximately 20 years, which well matches the time interval between the artificial channel avulsion in 1996 and core sampling in 2015 that deduced an average sedimentation rate of 1.90 cm/yr.

4.2.2. Grain-size variation

Corresponding to the sediment characteristics, the top-to-bottom sediment compositions and median grain size of cores AC1, AC2 and AC3 can be divided into two stages as distinguished by the evident vertical differences in sedimentary features (Fig. 5a). Stage 1 (100–38 cm) of core AC1 was characterized by high contents of sand (50.22%) and silt (47.42%), and an extremely low clay content (2.36%); the median grain size was 63.97 μm . Stage 2 (the upper 38 cm in depth) of core AC1, representing the sedimentation within 20 years after the channel abandonment in 1996 (Fig. 5a), processes a sand content of 10.11%, and a silt and clay content of 79.64% and 10.25%, respectively. The median grain size was 27.64 μm . At stage 1 (43–27 cm) of core AC2, the sand fraction was dominant, with a mean content of 56.34%. The average silt and clay contents were 38.56% and 5.10%, respectively (Fig. 5b), and the median grain size was 52.40 μm . At stage 2 (27–0 cm) the sand content decreased sharply to 21.83%, while the silt fraction increased to 65.86% with increasing clay content, resulting in a decrease in the median grain size to 20.97 μm (Fig. 5b). Similar to AC1 and AC2, sediment compositions of the 50 cm long core AC3 is also divided into two stages with a boundary at depth of 20 cm below surface. The average fractions of sand, silt and clay changed from 66.12%, 29.97% and 3.90% at stage 1, to 29.27%, 62.00% and 8.72% at stage 2, respectively (Fig. 5c). The median grain size decreased correspondingly from 63.30 μm at stage 1 to 28.67 μm at stage 2 (Fig. 5c).

The grain-size distribution curves express grain-size populations and are useful to interpret the sedimentary environments. The averaged distribution of the different stages of all three cores shows uni-modal distributions (Fig. 6). For each core, the maximum grain size percentage decreased sharply from stage 1 to stage 2. For instance, core AC1 shows the maximum-percentage population changed from 68.15 μm at stage 1 to 34.09 μm at stage 2 (Fig. 6). For the same stage in different cores, the peaks in the grain size distribution curves show a landward increase (i.e. from the core AC1 to AC3), particularly for stage 1 deposits, indicating that the sediment fines and is less sorted progressing downstream (Fig. 6).

4.2.3. Profiles of TOC and N-alkanes data analysis

TOC over the entire sediment samples of core AC1 showed a slight upward increasing trend, with a fluctuation of 0.03–0.12% (Fig. 7a). At

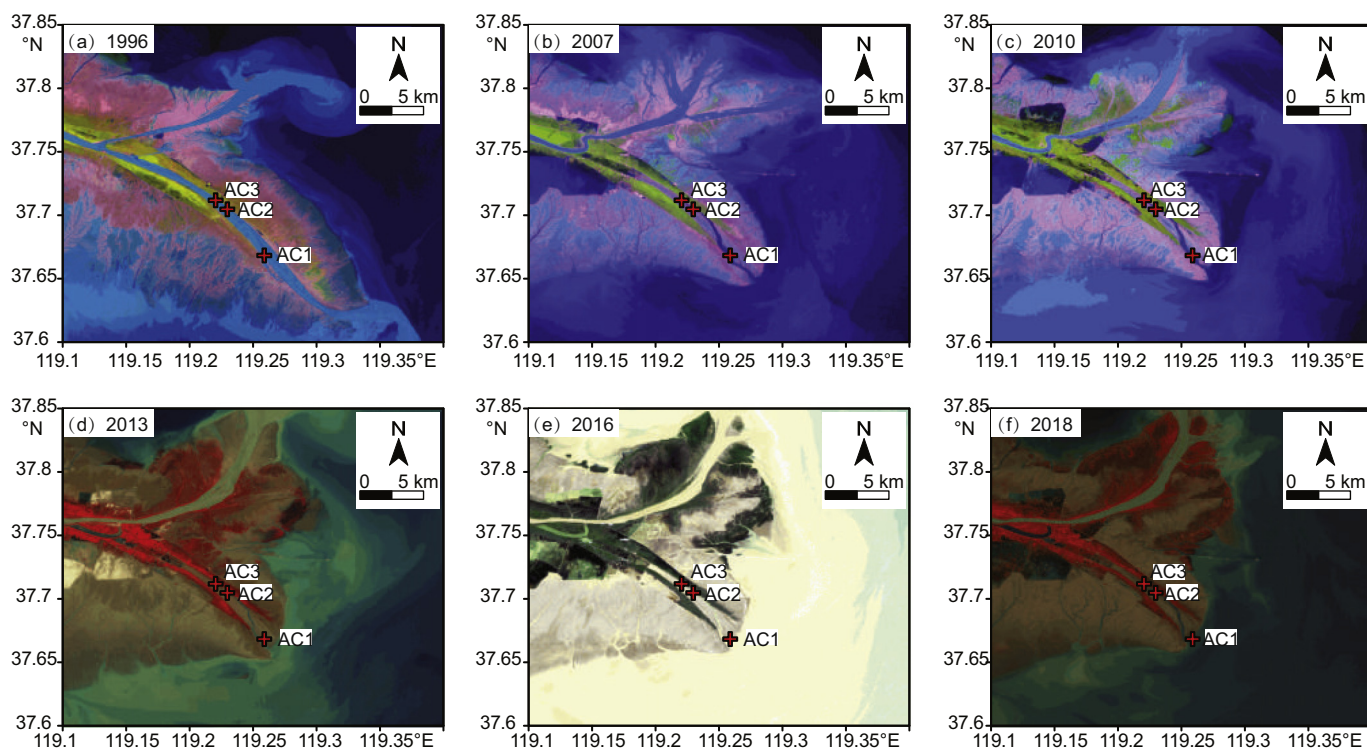


Fig. 2. Evolutions of the abandoned Qingshuigou channel lobe by Landsat images (<http://glovis.usgs.gov/>).

stage 1, TOC content varied between 0.03 and 0.08%, with a mean content of 0.05%. However, the mean value of TOC at stage 2 of core AC1 increased to 0.10% (Fig. 7a), together with significant contrast of grain-size composition (Fig. 7a). The TAR value of n-alkanes of sediment samples at stage 1 (mean of 94.48) is one order of magnitude higher than that at stage 2 (Fig. 7b). The L/H values display an opposite pattern with the TAR values (Fig. 7c). The mean L/H was as low as 0.02 at the bottom, increasing to 0.22 at the upper segment with considerable fluctuations (Fig. 7c). Fig. 8 shows n-alkanes distributions for core AC1 at different depths that were randomly chosen from different stages. The n-alkanes compositional patterns at depth of 80 cm

exhibited a typical unimodal distribution pattern centered at C₂₄-C₃₀ (Fig. 8) without odd/even predominance (CPI = 1.02). The n-alkanes distribution of sediment at 15 cm included two apparent populations (Fig. 8). The long-chain n-alkanes are concentrated in the range from C₂₉ to C₃₅, with a maximum at C₂₉ and C₃₁ (Fig. 8). The CPI value of C₂₅-33 homologues was 3.60, showing a significant odd to even carbon preference. The short-chain n-alkanes had a range from C₁₃ to C₂₀, with a maximum value occurring at C₁₆ (Fig. 8).

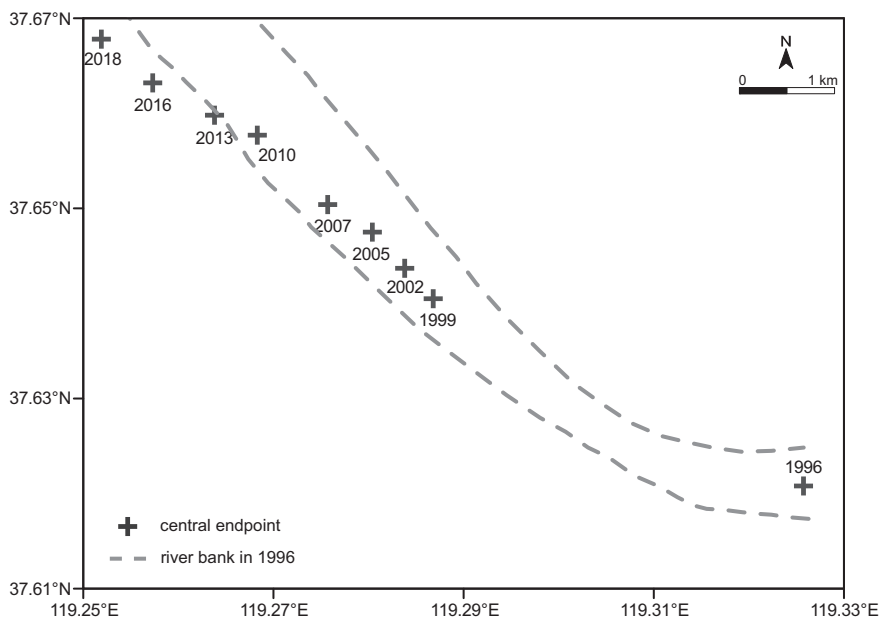


Fig. 3. Central endpoint of the abandoned Qingshuigou river mouth in different years.

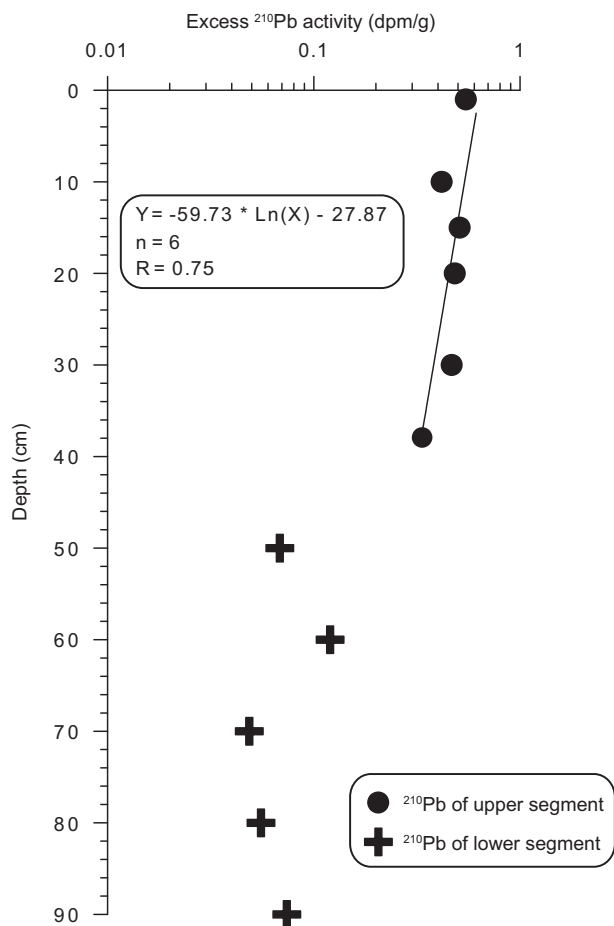


Fig. 4. Profile of excess ²¹⁰Pb activity in core AC1.

4.3. Regime of sediment transport

The SSC and tidal currents at station S1 located near the abandoned river mouth, for both summer and winter observations are shown in Fig. 9. On August 06, 2017, a southerly wind with velocity < 2.39 m/s blew over the study area. The tidal currents at the abandoned river mouth were reciprocating flows: northward during the flood tide but southward during the ebb tide (Fig. 9a). The flood tide lasted for ~6 h with a mean velocity of 13.70 cm/s, while the ebb tide lasted for ~4 h with a mean velocity of 18.56 cm/s (Fig. 9a), which presents an apparent tidal asymmetry. During the summer observation, the SSC fluctuated between 22.20 mg/L and 59.10 mg/L (Fig. 9b). The mean SSC during the flood tide was 39.78 mg/L, then decreased to 31.35 mg/L during the ebb tide. As a result, the SSF (suspended sediment flux) across the abandoned river mouth could have intruded the abandoned channel with a net value of 1.94 g/m/s in the NS direction, and 0.18 g/m/s in the EW direction, respectively. Considering the location of the time-series station (S1, Fig. 1b), the NS and EW directions indicate the sediment into channel and to the bank, respectively.

During the winter cruise, the northerly wind prevailed but with largely varying speed. It exceeded 12.84 m/s on March 15 and then weakened to 5.32 m/s on March 16, 2018. The tidal current flowed northwestward during the flood tide and southeastward during the ebb tide (Fig. 9c). The mean velocity was 50.41 cm/s during the flood tide and 51.57 cm/s during the ebb tide during the first tidal cycle, while the current velocity was only 12.44 cm/s with a fluctuation of 0.97–28.41 cm/s during the second cycle. The duration of the flood tide was ~5.5 h and ~3.3 h in the first and second cycles, respectively, shorter than those for the ebb tide (Fig. 9c). Comparing to the summer observation, the SSC in winter was extremely high (Fig. 9d), especially in the first tidal cycle after the passage of a gale. The mean SSC was 1264.16 mg/L and 503.39 mg/L in the first and second cycle, respectively (Fig. 9d). Besides an intrusion pattern along NS-direction, the SSF in the winter observation also displayed a considerable eastward transport. The northern and eastern SSF in the first tidal cycle was 19.28 g/m/s and 258.31 g/m/s, and then decreased to 2.42 g/m/s and 18.72 g/m/s in the second cycle, respectively. Comparing to the summer observation, the NS and EW directions of SSF was one or two orders higher in magnitude, respectively.

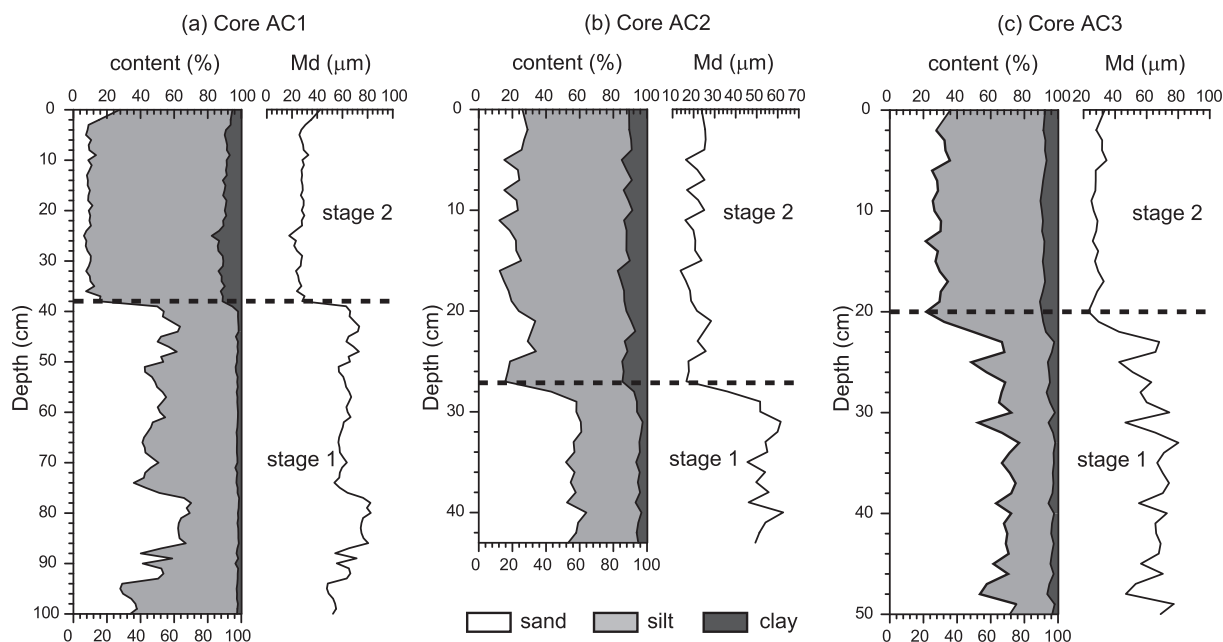


Fig. 5. Sediment composition and median grain size of (a) core AC1, (b) core AC2 and (c) core AC3. Dashed black line indicates change from fluvial sedimentation (below) to tidal sedimentation (above).

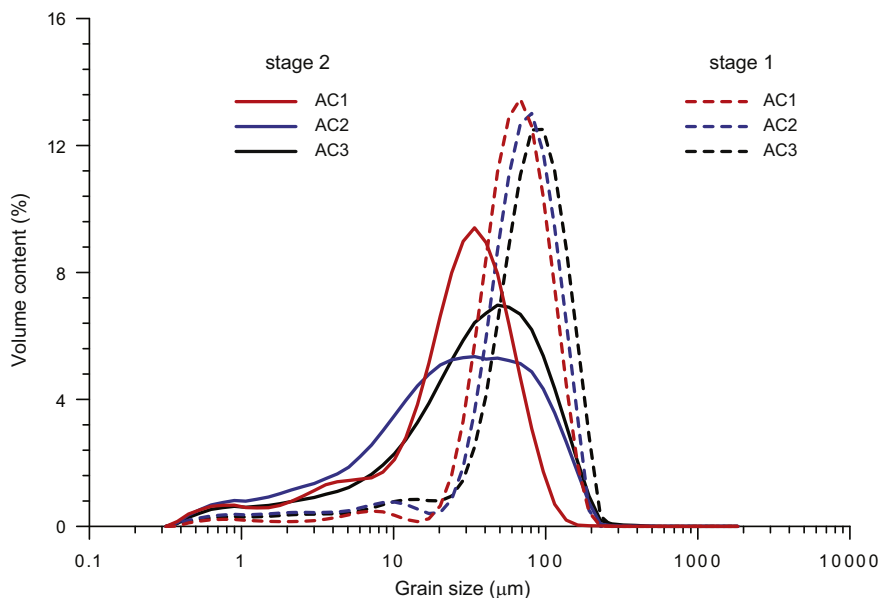


Fig. 6. Grain-size distribution curves of mean values at stage 1 (fluvial) and stage 2 (marine) for different cores.

5. Discussion

5.1. Evolution of the abandoned Qingshuigou river channel

Since 1976, when the Yellow River was diverted from the Diaokou course to the Qingshuigou course, the active delta lobe prograded seaward rapidly due to sufficient supply of riverine sediment (Wu et al., 2017). During this period, a large amount of coarse sediment containing a high proportion of sand and silt could have accumulated to form a fairly uniform bed texture (Stage 1 in Fig. 5). This was confirmed by geochemical evidences including low TOC, high TAR and low L/H values of n-alkanes (Fig. 7). The abundance of mid- and long-chain n-alkanes (i.e. C₂₄-C₃₀) illustrates a mixed source of aliphatic hydrocarbons, including floating/submerged macrophytes, and terrestrial and emergent plants, among which the terrestrial plants are the

predominant origin (Fig. 8; Ficken et al., 2000). The low CPI value at stage 1 suggests an input of petroleum hydrocarbons from the nearby oilfield, which is similar to the surface sediments of the active Qing 8 river channel (Wang et al., 2018).

Since abandonment in 1996, the Qingshuigou channel has been receiving a considerable amount of sediment from the nearshore re-suspension rather than from the river supply, resulting in continuous channel infilling. However, the in-channel sediment contains little sand and is much finer than the underlying antecedent channel bed (Fig. 5). Compared to the pre-existing bed deposits, infilling sedimentation is characterized by high content of organic matter, low TAR value and high L/H value (Fig. 7a), all suggesting a dominant contribution of aquatic plants (Meyers, 1997). In general, contrasting relationships exist between the concentrations of organic matter and sediment grain size (Lin et al., 2002). But in estuarine zones, organic matter can also be

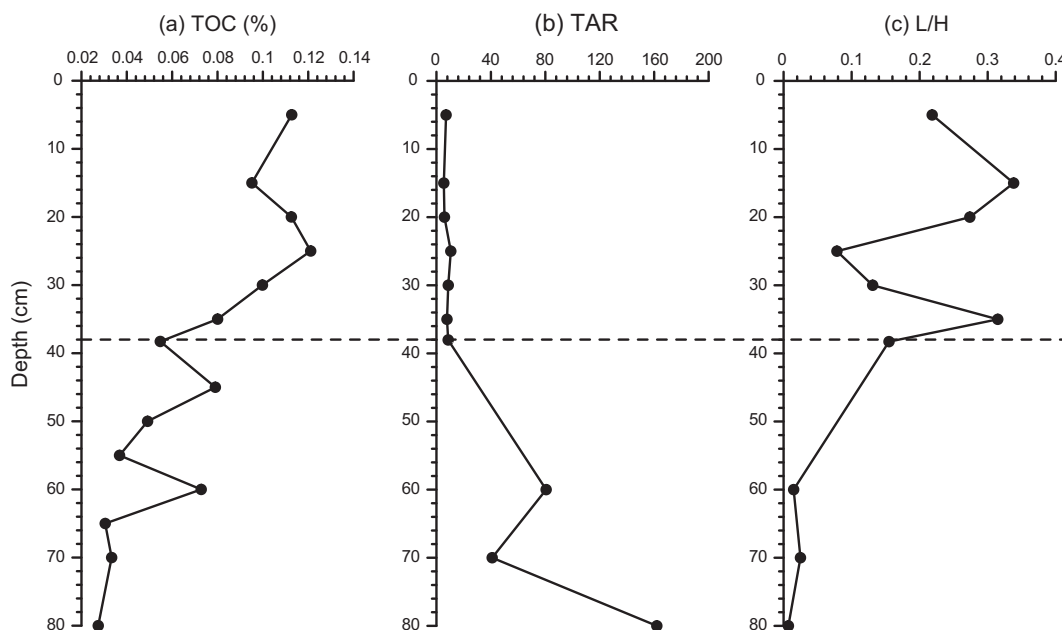


Fig. 7. Depth profile of (a) TOC content, (b) TAR value and (c) L/H value of core AC1. Dashed black line indicates change from fluvial sedimentation (below) to tidal sedimentation (above).

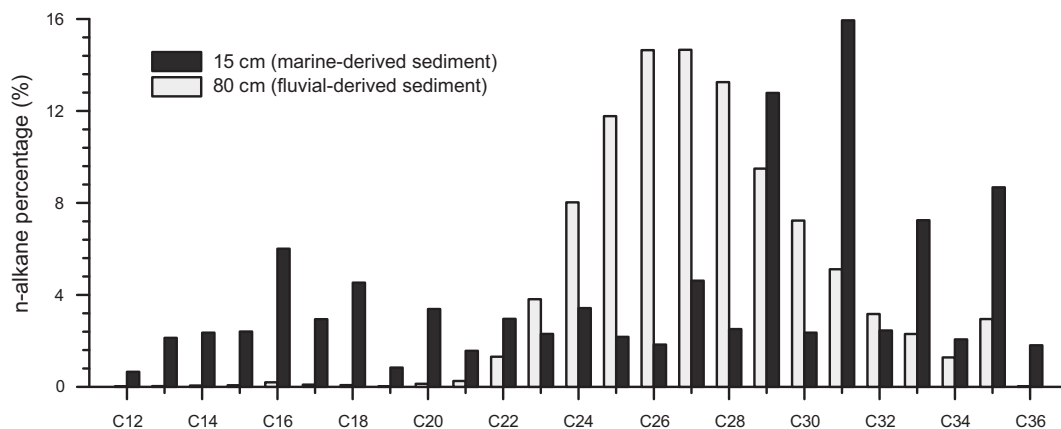


Fig. 8. Molecular distribution of n-alkanes at different stages of the core AC1.

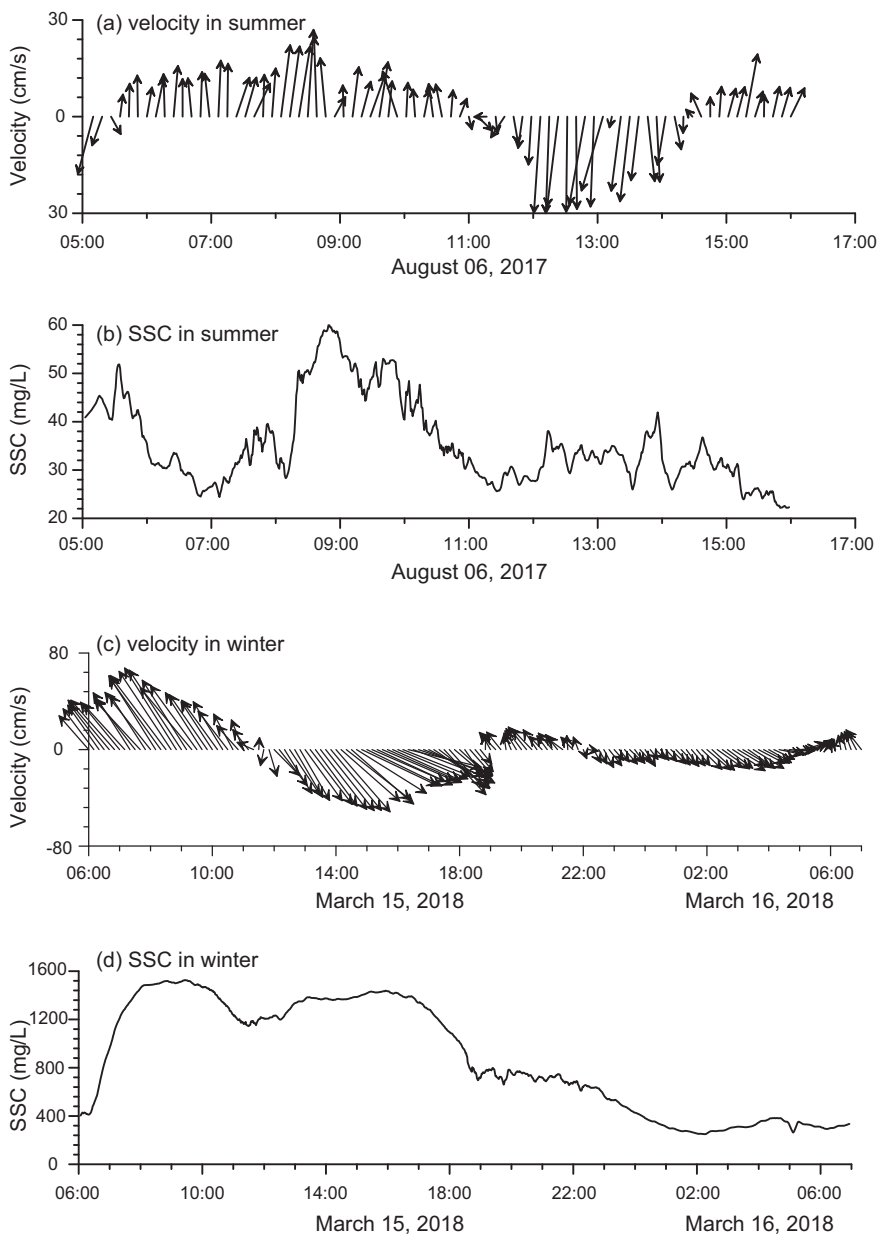


Fig. 9. Temporal variations of (a, c) velocity and (b, d) SSC, in summer and winter.

delivered from a marine source (Dinakaran and Krishnayya, 2011). The molecular distributions of n-alkanes confirmed that before the channel abandonment the terrestrial vascular plants are the dominant source for the organic carbons as indicated by the significant odd carbon number predominance of long-chain n-alkanes (Fig. 8; Aboul-Kassim and Simoneit, 1996). In contrast, the sources of organic carbon preserved in the abandoned channel at stage 2 seemed to be a mixture of marine organic matter and terrestrial aquatic plants since the concentration peaks of both long-chain and short-chain n-alkanes seemed to be evident (Fig. 8). Except for the in-channel perseveration of marine organic matters (short-chain n-alkanes) along with sedimentation (Dinakaran and Krishnayya, 2011), the growth of *Suaeda salsa* on the newly deposited bank of the abandoned channel (e.g. Zhang et al., 2018) might be partially responsible for contribution of organic matter from the terrestrial aquatic plants (Fig. 8). The fining trend of grain size, increase of organic matter and increased contribution of marine organic material at stage 2 of core AC1 (Figs. 5 and 7) are in good conformity.

The sedimentological and geochemical datasets indicate that the accumulation of fine-grained and organic-rich sediment dominates infilling process of the abandoned channel (Fig. 5). Meanwhile, a notable trend of seaward thickening of sediment accumulation from the middle to lower reach was identified (i.e., 20, 27, 38 cm for cores AC3, AC2, and AC1, respectively, Fig. 5). Continuous sedimentation, in combination with the gradual establishment of vegetation (Zhang et al., 2018), forced the channel to convert from a riverine environment to a tide-dominated environment (Steiger et al., 2001).

5.2. Influential factors on infilling of the abandoned channel

The downstream flow of the Yellow River into the Qingshuigou channel was blocked by a man-made dyke in 1996, rendering the abandoned course completely disconnected from the main (primary) fluvial channel (Zheng et al., 2018). Therefore, the abandoned river mouth is the only passage for sediment delivery to the channel (Veen et al., 2005). The imbalances in flow velocity and SSC arising during the flood and ebb tides produced a net landward sediment transport, which plays a critical role in infilling of the abandoned channel (Fig. 9). Such circumstance was similar to downstream tract of those tide-influenced active channels where tidal processes tend to produce a landward sediment transport, especially during dry season with low/no flow (Nowacki et al., 2015).

The coastal dynamics in the study area has distinct seasonal variability due to the impacts from monsoonal activities (Yang et al., 2011). During the summer and autumn seasons, the marine environment is less energetic due to weak wind, corresponding to less active sediment resuspension along the Yellow River delta (Wang et al., 2014). As a result, a majority of the river-delivered sediment is preferentially deposited at the active Yellow River mouth, and therefore only a minor fraction could be transported into the abandoned river mouth (Wu et al., 2015). Additionally, both the nearshore sediment concentration and the SSF into the abandoned channel during the summer and autumn seasons are quantitatively low (Fig. 9). Alternatively, during the winter and spring seasons, strong northerly winds prevailing over the Bohai Sea produce significant wave actions along the Yellow River delta, resulting in active resuspension of coastal sediment that can enter the abandoned river mouth (Yang et al., 2011; Wang et al., 2014). Therefore, the SSC near the Qingshuigou mouth becomes significantly higher in the winter-spring seasons and particularly pronounced during storm events (Wang et al., 2006). Highly turbid water, in combination with the enhanced coastal currents (Liang et al., 2007), produces a landward sediment flux into the abandoned channel, approximately one or two orders higher in magnitude than that in summer (Fig. 9). As a result, the winter season is a critical time window for the filling of the abandoned channel.

Gale and storm are frequent in winter season, accounting for nearly 16.44% of winter time in the past 10 years (Wu et al., 2019). Based on the width of the abandoned river mouth (~100 m) and limited time-

series observations at the abandoned river mouth in summer and winter seasons (Fig. 9), we roughly estimated that $\sim 11.2 \times 10^3$ t of sediment could be transported into the abandoned Qingshuigou channel annually, together with 11.59 t/yr of organic carbon (0.10% of TOC content in average, Fig. 7a). Given the complex impacts from variable factors such as tide, waves and channel geometry, more investigations on sediment cores and sediment dynamics are still needed in order to better quantify the filling flux into the abandoned channel.

It is noteworthy that the abandoned channel is not merely a 'sink' (i.e., solely receiving sediment input) during the winter season. Storm waves and enhanced near-shore currents induced severe erosion as the abandoned river mouth retreated landward continuously (Fig. 2; Wu et al., 2017). Under such situation, the abandoned channel transitioned to be a sediment source in marine environment, as the resuspended sediment could be transported by coastal currents over a long distance to the adjacent epicontinental sea (Zhang et al., 1990; Qiao et al., 2017). The protuberant topography of the abandoned river mouth renders the western bank of the channel (facing the strong waves and currents) to be easily eroded (Yang et al., 2011). Then this eroded sediment may be transported by eastward ebb currents; as a consequence, the combined effect of erosion on the west bank and depositing on the east bank eventually induced the lateral migration of the tidal inlet (Fig. 3).

Although the spring/neap tidal variation is not examined in this study, it should be regarded as another influencing factor on abandoned channel fill by enhanced current and increasing sediment concentration as well as depth of inundation by sediment-laden tidal water entering the abandoned channel (Kvale, 2006; Gray et al., 2016). Moreover, the seaward fining trend of sediment at Stage 2, as noted based on the three cores collected from middle and lower reach of the abandoned Qingshuigou channel (Fig. 6), might illustrate a contribution of seaward ebb tidal currents, in terms of physically sorting the channel fill deposits. As it fills over time, changes in depth, width and slope of the abandoned Qingshuigou channel are expected to alter the hydro-sedimentological connection and thereby influence the geomorphic and sedimentary evolution of this abandoned channel (e.g. upward fining/coarsening in the tide-derived deposits; Toonen et al., 2012). The character of the sediment cores discussed in this study, as well as deposits described in previous publications, could be helpful for illuminating stratigraphic distinctions of sediments comprising antecedent channel deposits, and sediment that subsequently fills the abandoned channel. Nevertheless, the accumulation rate of the abandoned channel should gradually decrease with time due to the morphological constraints on the hydro-sedimentological connectivity to both the main channel and/or marine system (Fisk, 1947; Constantine et al., 2010). The interactions between changing morphology of the abandoned channel and hydrodynamics over time are complicated and therefore more investigations using both observations and modeling efforts are needed in future.

5.3. Conceptual model for infilling process of tide-dominated abandoned channel

By influencing the apportionment of sediment and water to the abandoned channel, the bifurcation zone morphology, downstream channel slope and antecedent bars play a significant role in the geomorphic evolution of abandoned fluvial channels (Constantine et al., 2010; Dépret et al., 2017). Along with the growth of plug bars at the entrance of the abandoned channel, the hydro-sedimentological connectivity between abandoned channel and primary channel should be progressively weakened, due to the gradually elevated bed level resulting from the accumulation of fine-grained sediment (Toonen et al., 2012). Largely differing from previous fluvial environment, the tidal delivery of nearshore sediment into an abandoned river mouth has become critical to the sedimentary and geomorphological processes of the abandoned deltaic channel. Based on the case study of the abandoned Qingshuigou channel, a conceptual model for the infilling process of a tide-dominated abandoned channel is summarized (Fig. 10).

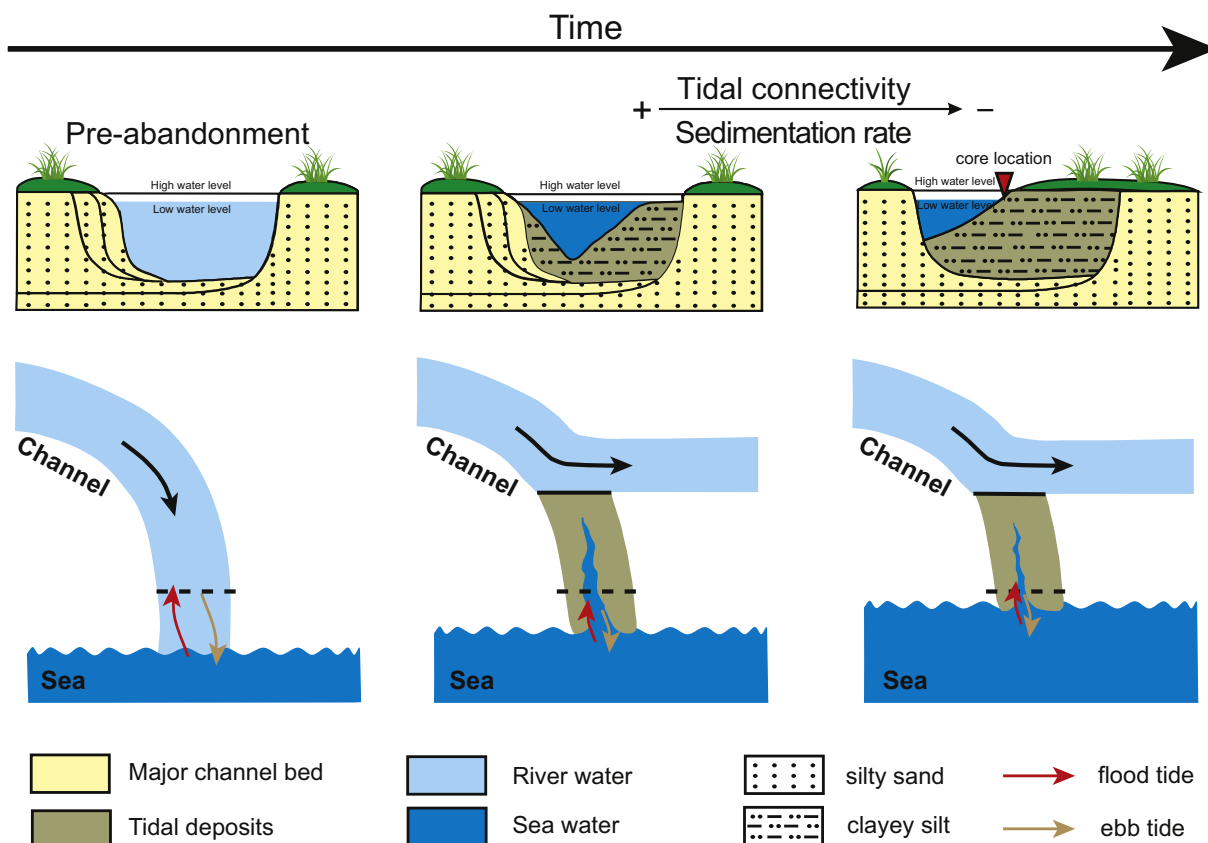


Fig. 10. Conceptual model of abandoned channel fill progression in purely tide-dominated system (modified after Gray et al., 2016).

Given that this particular channel never kept a connection to the main channel, there is no resistance provided by upstream-to-downstream fluvial discharge, and so the downstream-to-upstream propagating tide should more easily penetrate the abandoned channel. In other words, there is no oscillating fluvial and tidal water mixing, and so water and sediment movement into and out of the channel is purely driven by tides (Gray et al., 2016). The channel width near the abandoned river mouth was still wider than the upstream channel (Fig. 1b), somewhat like the active channel impacted by tidal processes (Gugliotta and Saito, 2019). The downstream entrance of the abandoned channel narrows gradually, but remains open due to tidal flow scouring (Fig. 10). Thus it is possible that, as a consequence of bi-directional tidal flow (flood and ebb tides), abandoned channels evolve could remain connected to a sediment-laden water source for a long period of time.

The abandoned channel fill deposits are mainly clayey-silt, rich in organic matter, overlying the sandy fluvial deposits (Fig. 10). There is no upward fining trend noted in the grain size of these discrete deposits (Stage 2 in Fig. 5). Although riverine sediment cannot enter the abandoned channel, sediment from the active river mouth could be transported to the abandoned river mouth by tidal currents (Wu et al., 2015). Therefore, to some extent, the infilling sediment of a purely tide-dominated abandoned channel could contain a signature of active fluvial sediment, although this supposition is not supported by the data and analyses presented herein for the Qingshuigou lobe. Additionally, the channel fill deposits could also preserve information about variations in the marine environment, such as marine productivity and/or marine pollutants. Furthermore, as the outer part of abandoned channel facing the robust wave and current environment of the sea is eroded, this material can be a sediment source for the adjacent epicontinental sea. This is another uniqueness of abandoned deltaic channels compared to their purely fluvial counterparts. Correspondingly, the length of abandoned channel is shortened as the lobe recedes, with lateral

migration of the tidal inlet, which shallows and narrows the abandoned channel thereby limiting tidal sediment flux over time (Fig. 10).

5.4. Comparison with other deltaic river channels

Due to artificial cut off by a man-made dyke, the abandoned Qingshuigou channel, a river channel located on a river-dominated delta, has converted to be a purely tide-dominated channel as hypothesized by Gugliotta and Saito (2019). Correspondingly, the river mouth retreated landward significantly with an average rate of 0.4 km/yr, from fast seaward protruding with a mean rate of 1.3 km/yr before abandonment (Wu et al., 2017). The retreat of this past river-dominated deltaic channel is even faster than part of tide-dominated deltaic channels, e.g. the Ganges-Brahmaputra river system (< 0.2 km/yr; Brammer, 2014) and the Mekong River (0.02–0.05 km/yr; Li et al., 2017), and part of wave-dominated deltaic channels, for example, the Nile River (0.01–0.1 km/yr; Frihy and Komar, 1993). Such retreat clearly shows a ghastly destructive process of a sediment-laden river induced by artificial closure of sediment supply.

For those tide-dominated deltaic channels which are partially or fully connected to main channels, sediment export driven by fluvial processes and sediment import driven by tidal processes dominate the local stratigraphy. In these channels, the channel fill architectures therefore record quasi-annual scale fluvial/tidal deposition couplets, which mainly consist of sandier, fluvial deposits with millimeter-scale laminations of finer, tidal deposits (Gray et al., 2018; Gugliotta and Saito, 2019). Such stratigraphic patterns dominated by alternating mud and sand beds are widely seen, in both the active tide-dominated channels (e.g. the Mekong River, Gugliotta et al., 2017), the Ganges-Brahmaputra river system (Wilson and Goodbred, 2015) and the abandoned tide-dominated channels (e.g. the Salinas River, Gray et al., 2018). In this case, however, there are no sand-mud alternations in

abandoned channel fill deposits (Fig. 5). Furthermore, due to a lack of riverine sediment supply during flood periods, the channel infilling rate of the abandoned Qingshuigou channel is much lower than those abandoned channels influenced by both fluvial and tidal forces, such as the Eel River (5 cm/yr, Gray et al., 2016). Besides, the abandonment of distributary channels of deltas occurs not only by avulsion, but also by delta progradation (Tamura et al., 2012). In those abandoned channels caused by delta progradation, coastal erosion is also much slower than that in this case (Dai et al., 2016).

6. Conclusions

Based on sedimentary records and hydrographic data, sedimentary architecture and dynamics of the abandoned Qingshuigou course, a purely tide-dominated abandoned channel, are documented in this study. In 1996, when an artificial diversion occurred, the abandoned Qingshuigou course was instantly disconnected from the main channel. Since then, it has received over 20 cm of in-channel sedimentation, with a seaward increasing trend in thickness along the channel axis from middle to lower reach. The abandoned channel fill deposits are much finer, possessing more organic matter than the underlying channel bed. As the abandoned river mouth is the only passage for sediment supplied to the abandoned channel, the filling process depends on imbalances in sediment flux (the product of water movement and SSC) during flood and ebb tides. Thus, the ability of sediment-laden tidal water to penetrate the downstream channel mouth has a critical control on the development of the abandoned channel. Comparing to those channels abandoned with a purely fluvial context, the downstream entrance of a tide-dominated channel could remain open due to scouring by tidal currents. Therefore, in general, the purely tide-dominated abandoned channel could be maintained for a relatively longer time period.

Severe erosion of the outer part of the abandoned channel, induced by dynamic waves and currents, gradually shorten the length of abandoned channel and cause the tidal inlet to migrate laterally; this is unique to tidally dominated channels and would not arise in abandoned systems experiencing fluvial forcing alone. The portion of eroded sediment could be transported from the delta front by marine currents and contributes as a sediment source to the adjacent epicontinental sea, while a portion of sediment could be transported by tides into the abandoned channel, contributing to its filling and development.

Declaration of competing interest

The authors declare that they have no known competing financial interests or personal relationships that could have appeared to influence the work reported in this paper.

Acknowledgement

The authors are grateful to Rice University personnel, specifically, Andrew Moodie and Tian Dong, for their participating in the fieldwork conducted in the abandoned Qingshuigou channel. This research was primarily funded by the Ministry of Science and Technology of the People's Republic of China (Nos. 2016YFA0600903 and 2017YFC0405502) and Shandong Provincial Natural Science Foundation (No. ZR2018BD028). Support was also received from the National Science Foundation of China (NSFC, grants Nos. 41806101, 41525021, 41530966 and U1606401) and the Laboratory for Marine Geology, Qingdao National Laboratory for Marine Science and Technology (grant No. MGQNL201709). JAN gratefully acknowledges the NSF (USA) for support through EAR grant no. 1427262, "Coastal SEES Collaborative Research: Morphologic, Socioeconomic, and Engineering Sustainability of Massive Anthropogenic Coastal Deltas: The Compelling Case of the Huanghe Delta."

Data availability

The datasets including grain size, geochemical data, chronological data, suspended sediment concentration and current reported in this paper have been uploaded into Figshare (DOI: <https://doi.org/10.6084/m9.figshare.9758339>). Satellite images used in this study are freely available from Earth Resources Observation and Science Center (<http://glovis.usgs.gov/>).

References

- Aboul-Kassim, T.A.T., Simoneit, B.R.T., 1996. Lipid geochemistry of surficial sediments from the coastal environment of Egypt I. Aliphatic hydrocarbons — characterization and sources. *Mar. Chem.* 54, 135–158.
- Allen, G.H., Pavelsky, T.M., 2018. Global extent of rivers and streams. *Science* 361, 585.
- Bakker, M.H.N., 2009. Transboundary river floods: examining countries, international river basins and continents. *Water Policy* 11, 269–288.
- Best, J., 2019. Anthropogenic stresses on the world's big rivers. *Nat. Geosci.* 12, 7–21.
- Bi, N., Yang, Z., Wang, H., Hu, B., Ji, Y., 2010. Sediment dispersion pattern off the present Huanghe (Yellow River) subdelta and its dynamic mechanism during normal river discharge period. *Estuarine Coastal and Shelf Science* 86, 352–362.
- Bi, N., Sun, Z., Wang, H., Wu, X., Fan, Y., Xu, C., Yang, Z., 2019. Response of channel scouring and deposition to the regulation of large reservoirs: a case study of the lower reaches of the Yellow River (Huanghe). *J. Hydrol.* 568, 972–984.
- Brammer, H., 2014. Bangladesh's dynamic coastal regions and sea-level rise. *Clim. Risk Manag.* 1, 51–62.
- Bray, E.E., Evans, E.D., 1961. Distribution of n-paraffins as a clue to recognition of source beds. *Geochim. Cosmochim. Acta* 22, 2–15.
- Constantine, J.A., Dunne, T., Piégay, H., and Mathias Kondolf, G., 2010. Controls on the alluviation of oxbow lakes by bed-material load along the Sacramento River, California. *Sedimentology* 57, 389–407.
- Dai, Z., Fagherazzi, S., Mei, X., Chen, J., Meng, Y., 2016. Linking the infilling of the North Branch in the Changjiang (Yangtze) estuary to anthropogenic activities from 1958 to 2013. *Mar. Geol.* 379, 1–12.
- Dépret, T., Riquier, J., Piégay, H., 2017. Evolution of abandoned channels: Insights on controlling factors in a multi-pressure river system. *Geomorphology* 294, 99–118.
- Dinakaran, J., Krishnappa, N.S.R., 2011. Variations in total organic carbon and grain size distribution in ephemeral river sediments in western India. *International Journal of Sediment Research* 26, 239–246.
- Ficken, K.J., Li, B., Swain, D.L., Eglinton, G., 2000. An n-alkane proxy for the sedimentary input of submerged/floating freshwater aquatic macrophytes. *Org. Geochem.* 31, 745–749.
- Fisk, H.N., 1947. Fine Grained Alluvial Deposits and Their Effects on Mississippi River Activity. U. S. Army: Corps of Engineers, Mississippi River Commission (Vicksburg), Waterways Exp. Sta 2, 82.
- Frihi, O.E., Komar, P.D., 1993. Long-term shoreline changes and the concentration of heavy minerals in beach sands of the Nile Delta, Egypt. *Mar. Geol.* 115, 253–261.
- Gray, A.B., Pasternack, G.B., Watson, E.B., Goñi, M.A., 2016. Abandoned channel fill sequences in the tidal estuary of a small mountainous, dry-summer river. *Sedimentology* 63, 176–206.
- Gray, A.B., Pasternack, G.B., Watson, E.B., 2018. Estuarine abandoned channel sedimentation rates record peak fluvial discharge magnitudes. *Estuar. Coast. Shelf Sci.* 203, 90–99.
- Gugliotta, M., Saito, Y., 2019. Matching trends in channel width, sinuosity, and depth along the fluvial to marine transition zone of tide-dominated river deltas: the need for a revision of depositional and hydraulic models. *Earth-Science Review* 191, 93–113.
- Gugliotta, M., Saito, Y., Nguyen, V.L., Ta, T.K.O., Nakashima, R., Tamura, T., Uehara, K., Katsuki, K., Yamamoto, S., 2017. Process regime, salinity, morphological, and sedimentary trends along the fluvial to marine transition zone of the mixed-energy Mekong River delta, Vietnam. *Cont. Shelf Res.* 147 (7–26).
- Guo, Z., Lin, T., Zhang, G., Zheng, M., Zhang, Z., Hao, Y., Fang, M., 2007. The sedimentary fluxes of polycyclic aromatic hydrocarbons in the Yangtze River Estuary coastal sea for the past century. *Sci. Total Environ.* 386, 33–41.
- Hu, L., Guo, Z., Feng, J., Yang, Z., Fang, M., 2009. Distributions and sources of bulk organic matter and aliphatic hydrocarbons in surface sediments of the Bohai Sea, China. *Mar. Chem.* 113, 197–211.
- Hu, L., Shi, X., Guo, Z., Wang, H., Yang, Z., 2013. Sources, dispersal and preservation of sedimentary organic matter in the Yellow Sea: the importance of depositional hydrodynamic forcing. *Mar. Geol.* 335, 52–63.
- Iglesias-Campos, A., Meiner, A., Bowen, K., and Ansong, J.O., 2015. Chapter 3 - coastal population and land use changes in Europe: challenges for a sustainable future, in: Baztan, J., Chouinard, O., Jorgensen, B., Tett, P., Vanderlinden, J.-P., and Vasseur, L. eds., *Coastal Zones*, Elsevier, 29–49.
- Kvale, E.P., 2006. The origin of neap-spring tidal cycles. *Mar. Geol.* 235, 5–18.
- Li, X., Liu, J.P., Saito, Y., Nguyen, V.L., 2017. Recent evolution of the Mekong Delta and the impacts of dams. *Earth-Science Review* 175, 1–17.
- Liang, B., Li, H., Lee, D., 2007. Numerical study of three-dimensional suspended sediment transport in waves and currents. *Ocean Eng.* 34, 1569–1583.
- Lin, S., Hsieh, I.J., Huang, K.M., Wang, C.H., 2002. Influence of the Yangtze River and grain size on the spatial variations of heavy metals and organic carbon in the East China Sea continental shelf sediments. *Chem. Geol.* 182, 377–394.
- Liu, F., Chang, X., Liao, Z., Yang, C., 2018. n-Alkanes as indicators of climate and

- vegetation variations since the last glacial period recorded in a sediment core from the northeastern South China Sea (SCS). *J. Asian Earth Sci.* 117, 134–143.
- Meyers, P.A., 1997. Organic geochemical proxies of paleoceanographic, paleolimnologic, and paleoclimatic processes. *Org. Geochem.* 27, 213–250.
- Nowacki, D.J., Ogston, A.S., Nittrouer, C.A., Fricke, A.T., Van, P.D.T., 2015. Sediment dynamics in the lower Mekong river: transition from tidal river to estuary. *Journal of Geophysical Research: Oceans* 120, 6363–6383.
- Ogston, A.S., Allison, M.A., Mullarney, J.C., Nittrouer, C.A., 2017. Sediment- and hydrodynamics of the Mekong Delta: from tidal river to continental shelf. *Cont. Shelf Res.* 147, 1–6.
- Qiao, S., Shi, X., Wang, G., Zhou, L., Hu, B., Hu, L., Yang, G., Liu, Y., Yao, Z., Liu, S., 2017. Sediment accumulation and budget in the Bohai Sea, Yellow Sea and East China Sea. *Mar. Geol.* 390, 270–281.
- Saito, Y., Yang, Z., Hori, K., 2001. The Huanghe (Yellow River) and Changjiang (Yangtze River) deltas: a review on their characteristics, evolution and sediment discharge during the Holocene. *Geomorphology* 41, 219–231.
- Shi, C., Dian, Z., You, L., 2002. Changes in sediment yield of the Yellow River basin of China during the Holocene. *Geomorphology* 46, 267–283.
- Steiger, J., Gurnell, A.M., Petts, G.E., 2001. Sediment deposition along the channel margins of a reach of the middle River Severn, UK. *Regulated Rivers. Research & Management* 17, 443–460.
- Syvitski, J.P.M., Saito, Y., 2007. Morphodynamics of deltas under the influence of humans. *Glob. Planet. Chang.* 57, 261–282.
- Syvitski, J.P.M., Kettner, A.J., Overeem, I., Hutton, E.W.H., Hannon, M.T., Brakenridge, G.R., Day, J., Vörösmarty, C., Saito, Y., Giosan, L., Nicholls, R.J., 2009. Sinking deltas due to human activities. *Nat. Geosci.* 2, 681.
- Tamura, T., Saito, Y., Nguyen, V.L., Ta, T.K.O., Bateman, M.D., Matsumoto, D., Yamashita, S., 2012. Origin and evolution of inter-distributary delta plains; insights from Mekong river delta. *Geology* 40, 303–306.
- Toonen, W.H.J., Kleinhans, M.G., Cohen, K.M., 2012. Sedimentary architecture of abandoned channel fills. *Earth Surf. Process. Landf.* 37, 459–472.
- Veen, J. van, Spek, A.J.F. van der, Stive, M.J.F., and Zitman, T., 2005. Ebb and flood channel systems in the Netherlands tidal waters. *J. Coast. Res.* 21, 1107–1120.
- Wang, H., Yang, Z., Li, G., Jiang, W., 2006. Wave climate modeling on the abandoned Huanghe (Yellow River) delta lobe and related deltaic erosion. *J. Coast. Res.* 22, 906–918.
- Wang, H., Bi, N., Saito, Y., Wang, Y., Sun, X., Zhang, J., Yang, Z., 2010. Recent changes in sediment delivery by the Huanghe (Yellow River) to the sea: causes and environmental implications in its estuary. *J. Hydrol.* 391, 302–313.
- Wang, H., Wang, A., Bi, N., Zeng, X., Xiao, H., 2014. Seasonal distribution of suspended sediment in the Bohai Sea, China. *Cont. Shelf Res.* 90, 17–32.
- Wang, H., et al., 2017. Impacts of the dam-orientated water-sediment regulation scheme on the lower reaches and delta of the Yellow River (Huanghe): a review. *Glob. Planet. Chang.* 157, 93–113.
- Wang, S., Liu, G., Yuan, Z., Da, C., 2018. n-Alkanes in sediments from the Yellow River Estuary, China: occurrence, sources and historical sedimentary record. *Ecotoxicology and Environmental Safety* 150, 199–206.
- Wetzel, R.G., 2001. 3 - rivers and lakes—their distribution, origins, and forms. In: Wetzel, R.G. (Ed.), *Limnology*, Third edition. Academic Press, San Diego, pp. 15–42.
- Wilson, C.A., Goodbred, S.L., 2015. Construction and maintenance of the Ganges-Brahmaputra-Meghna delta: linking process, morphology, and stratigraphy. *Annu. Rev. Mar. Sci.* 7, 67–88.
- Wu, X., Bi, N., Yuan, P., Li, S., Wang, H., 2015. Sediment dispersal and accumulation off the present Huanghe (Yellow River) delta as impacted by the water-sediment regulation scheme. *Cont. Shelf Res.* 111, 126–138.
- Wu, X., Bi, N., Xu, J., Nittrouer, J.A., Yang, Z., Saito, Y., Wang, H., 2017. Stepwise morphological evolution of the active Yellow River (Huanghe) delta lobe (1976–2013): dominant roles of riverine discharge and sediment grain size. *Geomorphology* 292, 115–127.
- Wu, X., Wu, H., Wang, H., Bi, N., Duan, H., Wang, C., Bian, C., Xu, J., 2019. Novel, repeated surveys reveal new insights on sediment flux through a narrow strait, Bohai, China. *Journal of Geophysical Research: Oceans* 124, 6927–6941.
- Xue, C., 1993. Historical changes in the Yellow River delta, China. *Mar. Geol.* 113, 321–330.
- Yang, Z., Ji, Y., Bi, N., Lei, K., Wang, H., 2011. Sediment transport off the Huanghe (Yellow River) delta and in the adjacent Bohai Sea in winter and seasonal comparison. *Estuar. Coast. Shelf Sci.* 93, 173–181.
- Zhang, J., Wen Huang, W., Chong Shi, M., 1990. Huanghe (Yellow River) and its estuary: sediment origin, transport and deposition. *J. Hydrol.* 120, 203–223.
- Zhang, S., Bai, J., Wang, W., Huang, L., Zhang, G., Wang, D., 2018. Heavy metal contents and transfer capacities of *Phragmites australis* and *Suaeda salsa* in the Yellow River Delta, China. *Physics and Chemistry of the Earth, Parts A/B/C* 104, 3–8.
- Zheng, S., Han, S., Tan, G., Xia, J., Wu, B., Wang, K., Edmonds, D.A., 2018. Morphological adjustment of the Qingshuigou channel on the Yellow River Delta and factors controlling its avulsion. *Catena* 166, 44–55.
- Zhou, Y., Huang, H.Q., Nanson, G.C., Huang, C., Liu, G., 2015. Progradation of the Yellow (Huanghe) River delta in response to the implementation of a basin-scale water regulation program. *Geomorphology* 243, 65–74.